Fault tolerant back-to-back converter topology for wind turbine with Doubly Fed Induction Generator

Arnaud Gaillard, Shahram Karimi, Philippe Poure, Shahrokh Saadate

Fault tolerant back-to-back converter topology for wind turbine with Doubly Fed Induction Generator

A. Gaillard[1], S. Karimi[1], P. Poure[2], S. Saadate[1]

Abstract – *This paper presents a novel fault tolerant converter topology for grid connected Wind Energy Conversion System (WECS) with Doubly Fed Induction Generator (DFIG). This topology allows fast fault detection and compensation of one of the semiconductors or drivers by using isolating and connecting devices. It is based on a unique redundant leg for both back to back converters. We present a new detection algorithm, robust to false fault detection due to semiconductor switching. Simulation results are presented cases on both back-to-back converters and both hyper and hypo synchronous conditions.*

Keywords: *Wind Turbine Generator, Fault Tolerant Converter, Fault detection, Fault compensation, Doubly Fed Induction Generator*

Nomenclature:

k (k = 1, 2, 3, 1′, 2′, 3′)	leg number
T_k	top IGBT switches
v_{kOm}	measured pole voltages
v_{kOes}	estimated pole voltages
V_{dc}	dc-link voltage
$int_k(t)$	time error signal
I_{ds}, I_{qs}, I_{dr} , I_{qr}	stator and rotor currents in the (d-q) reference frame
θ_s, θ_r	stator and rotor field angle
φ_{ds}, φ_{qs}, φ_{dr} , φ_{qr}	stator and rotor flux in the (d-q) reference frame
R_s, R_r	stator and rotor resistance
L_s, L_r	cyclic stator and rotor inductance
M	cyclic mutual inductance
T_{em}	electromagnetic torque
Tr	resistant torque
f	viscose torque coefficent
Ω	mechanical rotation speed
J	global inertia
p	pair poles number
V_s	RMS value of the grid voltage
P_{grid}	active power injected into the grid

I. Introduction

The demand for continuously available electronic power systems is increasing. Power systems are mostly feeding loads requiring non-stop and fault tolerant operation. WECS are typical application cases where the efficient production is directly linked to economic benefits [1]. The generator used in the studied WECS with DFIG is controlled by back to back converters to provide power to the grid. This distributed generation technology is one of the most used wind turbine generator in recently built wind farms [2]. DFIG present many advantages and is is the only variable speed wind turbine generator that does not require a full-size rated rotor side power converter to provide the grid with a constant frequency with unity power factor capability [2]. However, this WECS is highly sensitive to faults occurring at the back to back converters as well at the sensors. A sudden failure in one of the power switches or drivers decreases system performances and its effect can lead to hard failure. Hence, to reduce the failure rate and to prevent unscheduled shutdown, real-time fault detection, isolation, and compensation scheme should be adopted.

Recently, Shander-Mustapha and Slama-Belkohja studied current sensor failure in a DFIG wind turbine. They proposed a method to locate the faulty sensor and they proposed to reconfigure the controller [3]. More, the fault mode behaviour of static converters, protection and fault tolerant control of voltage source inverter systems has been covered in a large number of papers. Kastha and Bose [4] made a systematic investigation of the voltage source PWM inverter system for induction motor drives on various fault modes. However, they do not propose any method to identify faults. In [5]-[6] analysis of the current-vector trajectory is used to identify fault modes. Mendes and Cardoso [7] have suggested to use the average motor currents Park's vector monitoring, for diagnosing voltage source inverter faults in AC drives. All the methods previously discussed take at least one fundamental period to detect the fault occurrence. Special methods have been also developed to minimize the time between fault's occurrence and detection. Riberio et al. [8] proposed different techniques for fault detection in voltage source asynchronous machine drive systems. These techniques are a kind of knowledge based procedure and use extra

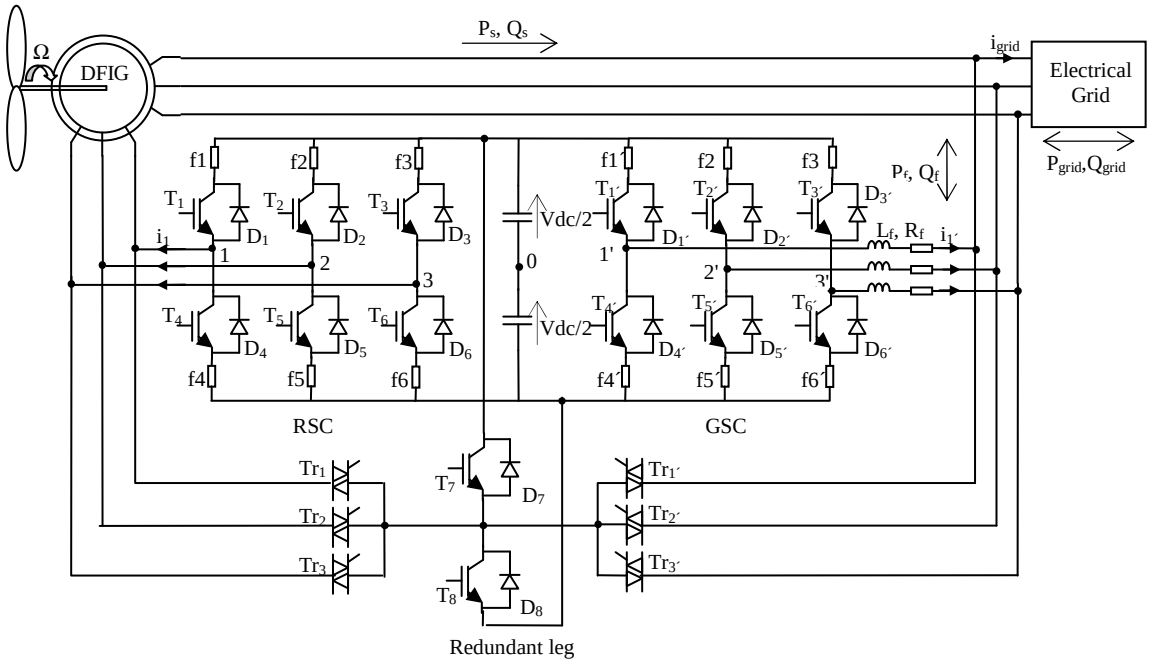

Fig. 1. Fault tolerant back-to-back converter topology.

sensors. With these techniques the fault is detected in one fourth of the fundamental cycle.

In this paper, we propose a new fault tolerant back-to-back converter topology. Then we detail a new fault identification and compensation method in both hyper and hypo synchronous conditions. First, we examine the response of the WECS in fault occurrence case for one semiconductor or driver of one of the two converters. Four cases are studied: the fault can either occur over the Grid Side Converter (GSC) or over the Rotor Side Converter (RSC) in both hyper or hypo synchronous mode. The approach introduced here minimizes the delay time between the fault occurrence and its diagnosis. This paper demonstrates the possibility to detect a faulty switch in less than 10 µs by using a "time criterion" instead of "voltage criterion". Finally, the proposed detection method is applied to the fault tolerant back-to-back converter topology. It only implements one redundant leg for any fault occurrence in the GSC or the RSC. Consequently, the back-to-back converter can still operate in nominal conditions even if a power semiconductor or a driver is faulty, in any wind speed conditions.

II. Fault tolerant topology

The studied WECS is based on a horizontal axis wind turbine and an indirect controlled DFIG with Maximum Power Point Tracking (MPPT) and pitch controls. Fig. 1 shows the fault tolerant topology. It is based on a back-to-back converter and a redundant leg composed of the switches T_7 and T_8. This leg will replace if necessary the faulty one of the other legs. When a fault has occurred in one of the semiconductors or drivers, the fault detection scheme detects and locates the fault and isolates the faulty leg. If the fault is an open-circuit, the isolation is implemented by removing the gate signal from both switches of the faulty leg. In short-circuit case, the faulty leg is isolated by very fast acting fuses; consequently, the short-circuit fault becomes an open-circuit fault after isolation of the faulty leg by the fuses. Then, in both cases, the reconfiguration scheme triggers the suited bidirectional switch T_{rk} in order to connect the faulty phase to the middle point of the redundant leg. In summary, in a fault case on the leg number k, the compensation is achieved by the following steps:

- Detection of the faulty leg (detailed in next section);
- Removing the switching orders of the two switching drivers of the faulty leg number k;
- Triggering of the suited bidirectional switch T_{rk};
- Using the switching orders of the faulty leg for the redundant one;
- Stopping the fault detection scheme.

III. Fast fault detection and identification principle

Power semi-conductors fault detection is based on the comparison between measured and estimated pole voltages. The estimated voltages can be expressed by:

$$v_{koes} = (2 \times S_k - 1)\frac{V_{dc}}{2} \quad (1)$$

Where S_k = {0, 1} is the switching pattern (opened or closed) for the top semi-conductor of the leg number k. The fault occurrence can be determined by analysing the voltage error obtained from the difference between the measured and estimated pole voltages.This voltage error is given by:

$$\varepsilon_{ko} = v_{kom} - v_{koes} \quad (2)$$

We suppose that the switches are ideal. With this supposition, in normal operation, the measured and estimated pole voltages are equal and thus their difference is zero.

In short circuit case, the fast acting fuse of the faulty leg first isolates the leg. Then, the faulty switch is opened and the fault detection also consists in an open-circuit fault. Consequently, only open-circuit fault will be studied in next sections.

In the following, the open-circuit fault in one of the top switches T_k is considered. The voltage error and the measured pole voltage are calculated analytically. An open circuit fault in the switch T_k reduces the pole converter topology to the equivalent circuit presented in the Fig. 2. In this circuit, the measured pole voltage and the voltage error for the phase k depend on the phase current i_k and the switching pattern S_{k+3} of the switch T_{k+3}.

Even though the estimated voltage, v_{koes}, depends only on the state of the switching pattern of the switch T_{k+3}, the measured pole voltage, v_{kom}, can be changed with the sign of the phase current i_k:

$$\text{If } i_k > 0 \text{ then } v_{kom} = -\frac{V_{dc}}{2} \quad (3a)$$

$$\text{If } i_k < 0 \text{ and } S_{k+3} = 1 \text{ then } v_{kom} = -\frac{V_{dc}}{2} \quad (3b)$$

$$\text{If } i_k < 0 \text{ and } S_{k+3} = 0 \text{ then } v_{kom} = \frac{V_{dc}}{2} \quad (3c)$$

Table 1 presents the voltage error. We demonstrated that the fault is detected only if $i_k > 0$ and $S_{k+3} = 0$ because in the other cases the leg number k operates correctly and thus the voltage error is zero.

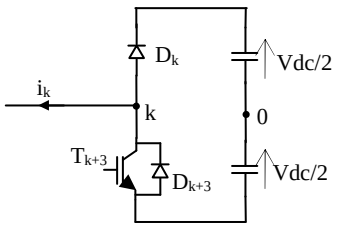

Fig. 2. Equivalent circuit for open circuit fault in the switch T_k.

TABLE I
VOLTAGE ERROR FOR OPEN CIRCUIT FAULT IN THE SWITCH

i_k	S_{k+3}	D_k	D_{k+3}	v_{kom}	v_{koes}	ε_{ko}
>0	*0*	Off	On	$-\frac{V_{dc}}{2}$	$\frac{V_{dc}}{2}$	$-V_{dc}$
>0	*1*	Off	On	$-\frac{V_{dc}}{2}$	$-\frac{V_{dc}}{2}$	0
<0	*0*	On	Off	$\frac{V_{dc}}{2}$	$\frac{V_{dc}}{2}$	0
<0	*1*	Off	Off	$-\frac{V_{dc}}{2}$	$-\frac{V_{dc}}{2}$	0

Same analysis can be used for the open-circuit fault in any one of the bottom switches. Thus with ideal switches consideration, the fault occurrence in each leg can be determined with a comparator that compares the measured and estimated pole voltages. However, in real case, because of turn-off and turn-on propagation time and interlock dead time generated by the switches drivers, the voltage error is not null in "healthy" conditions and constituted of pick during switching time. To avoid false fault detections due to power semi-conductors switching, we think of transforming the "voltage" error signal in a "time" error signal. Also, the time error signal $int_k(t)$ is achieved for each phase by first taking the absolute value of ε_{kO} (t), applying the result to a comparator with a value h and integrating the comparator output as presented in the Fig. 3. The output of the first comparator is equal to zero if $|\varepsilon_{kO}(t)| < h$ and equal to one if $|\varepsilon_{kO}(t)| \geq h$. Thus, the output of this comparator is a repetitive square waveform due to semi-conductors switching. The output of the integrator is equal to the time during which v_{kOm} and v_{kOes} are different, if integration is initialised to zero after each square waveform. Consequently, we detect the fault occurrence using a "time criterion" instead of "voltage criterion". To do this, we applied the integration result signal to a second comparator having a value T_f several times larger than switching time. By this way, we avoid false fault detections due to semiconductor switching and we can detect the fault in less than 10 µs. The resulting signal f_k from the fault detection scheme is used to isolate the faulty leg, to trigger the suited bidirectional switch T_{rk} and to stop the fault detection.

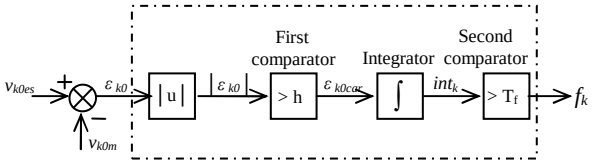

Fig. 3. Fault detection for the phase k.

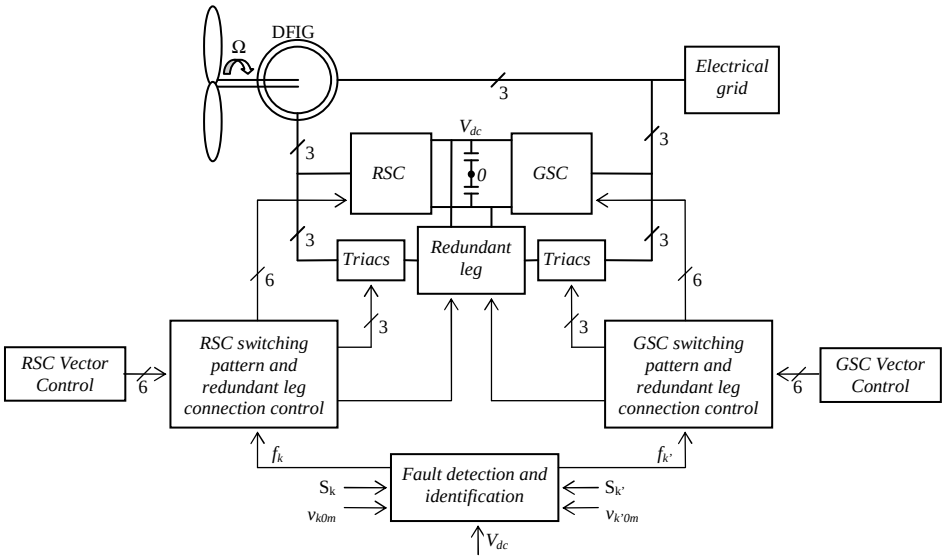

Fig. 4. Control of the Fault Tolerant System (k = 1, 2, 3).

IV. Control of the Fault Tolerant System

Fig. 4 shows the control principle for the fault tolerant WECS. In healthy conditions, the switching pattern for the RSC and GSC are defined by a vector control strategy, detailed in next section. The fault detection and identification bloc generates the f_k orders according the principle depicted in Fig. 3. The RSC or GSC switching pattern and the redundant leg connection control bloc manages the suited triac connection and the redundant leg switching pattern according to the detected faulty leg. In healthy conditions, the six outputs of the RSC or GSC control are directly applied to the RSC or GSC, whereas in fault case, only four of them are used for the RSC or GSC and the two others ones drive the redundant leg.

V. Vector Control of the DFIG

The studied DFIG is controlled to produce electrical power at constant frequency whatever wind and speed conditions. The stator of the DFIG is directly connected to the grid and the rotor is fed by two bi-directional converters (RSC and GSC) connected between the rotor and the grid. The indirect control method is based on regulating the active and reactive powers of the DFIG, by controlling the (d-q) rotor currents [9]-[10].

V.1. Modeling of the DFIG

We used the classical (d-q) modelisation in the Park reference frame [10]. The equations for a DFIG and a classical squirrel cage generator are identical, excepted the rotor voltages which are not null for the DFIG.

The stator and rotor voltages V_{ds}, V_{qs}, V_{dr} and V_{qr} in the (d-q) reference frame are defined by:

$$\begin{cases} V_{ds} = R_s I_{ds} + \dfrac{d}{dt}\varphi_{ds} - \dot{\theta}_s \varphi_{qs} \\ V_{qs} = R_s I_{qs} + \dfrac{d}{dt}\varphi_{qs} + \dot{\theta}_s \varphi_{ds} \\ V_{dr} = R_r I_{dr} + \dfrac{d}{dt}\varphi_{dr} - \dot{\theta}_r \varphi_{qr} \\ V_{qr} = R_r I_{qr} + \dfrac{d}{dt}\varphi_{qr} + \dot{\theta}_r \varphi_{dr} \end{cases} \quad (4)$$

With:

$$\begin{cases} \varphi_{ds} = L_s I_{ds} + M I_{dr} \\ \varphi_{qs} = L_s I_{qs} + M I_{qr} \\ \varphi_{dr} = L_r I_{dr} + M I_{ds} \\ \varphi_{qr} = L_r I_{qr} + M I_{qs} \end{cases} \quad (5)$$

After simplification, the equations (4) and (5) become:

$$\begin{cases} V_{ds} = R_s I_{ds} + \sigma L_s \dfrac{d}{dt} I_{ds} + E_{ds} \\ V_{qs} = R_s I_{qs} + \sigma L_s \dfrac{d}{dt} I_{qs} + E_{qs} \\ V_{dr} = R_r I_{dr} + \sigma L_r \dfrac{d}{dt} I_{dr} + E_{dr} \\ V_{qr} = R_r I_{qr} + \sigma L_r \dfrac{d}{dt} I_{qr} + E_{qr} \end{cases} \quad (6)$$

Where σ is defined by:

$$\sigma = 1 - \frac{M^2}{L_r L_s} \quad (7)$$

and E_{ds}, E_{qs}, E_{dr} and E_{qr} are the coupling terms between the d and q axes. Their expressions are given in Appendix.

The mechanical equation is:

$$T_{em} = T_r + f\Omega + J\frac{d\Omega}{dt} \tag{8}$$

The electromagnetic torque depends on the (d-q) flux and currents:

$$T_{em} = p\frac{M}{L_s}\left(I_{qr}\varphi_{ds} - I_{dr}\varphi_{qs}\right) \tag{9}$$

V.2. Control of the RSC

After Laplace transformation, the rotor voltages defined by the equation (6) become:

$$\begin{cases} V_{dr}(s) = R_r I_{dr}(s) + \sigma L_r s I_{dr}(s) + E_{dr}(s) \\ V_{qr}(s) = R_r I_{qr}(s) + \sigma L_r s I_{qr}(s) + E_{qr}(s) \end{cases} \tag{10}$$

With *s* the operator of Laplace.

The resulting bloc diagram for rotor voltages from equation (10) is presented in the Fig. 5. In this figure $F_{dr}(s)$ and $F_{qr}(s)$ are transfer functions for the rotor voltages and are expressed by:

$$F_{dr}(s) = F_{qr}(s) = \frac{1}{R_r}\cdot\frac{1}{1+\sigma\frac{L_r}{R_r}s} \tag{11}$$

To achieve an independent control of active and reactive power, we established the equations between the powers and the rotor variables of the DFIG. We choose to set the stator flux vector aligned with the d axe. Consequently:

$$\begin{cases} \varphi_{ds} = \varphi_s \\ \varphi_{qs} = 0 \end{cases} \tag{12}$$

The grid is assumed to be stable and consequently φ_{ds} is constant. By neglecting the stator resistance of the DFIG, we obtained :

$$\varphi_s = \frac{V_s\sqrt{3}}{\omega_s} \tag{13}$$

The active and reactive power of the DFIG can be expressed by :

$$\begin{cases} P_s = \sqrt{3}V_s I_{qs} \\ Q_s = \sqrt{3}V_s I_{ds} \end{cases} \tag{14}$$

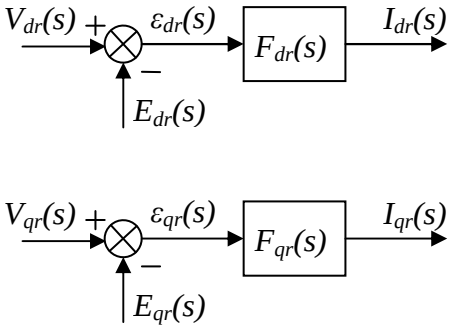

Fig. 5. Bloc diagram for the RSC voltages.

Or from the rotor currents by:

$$\begin{cases} P_s = -V_s\sqrt{3}\frac{M}{L_s}I_{qr} \\ Q_s = \frac{3V_s^2}{\omega_s L_s} - \frac{\sqrt{3}V_s M}{L_s}I_{dr} \end{cases} \tag{15}$$

The RSC control diagram presented in the Fig. 6 is directly established from the equations (15) of the DFIG model. We used a Proportional Integral corrector for the current control [11].

V.3. Control of the GSC

The model of the system (Fig. 7) is given by the following equation:

$$v_{123} = R_f i_{1'2'3'} + L_f\frac{d}{dt}i_{1'2'3'} + v_{1'2'3'} \tag{16}$$

R_f and L_f are respectively the resistance and inductor of the input filter. The Park model in the GSC (d-q) reference frame is given by:

$$\begin{cases} V_{ds} = R_f I_{d'} + L_f\frac{d}{dt}I_{d'} - \omega_s L_f I_{q'} + V_{d'} \\ V_{qs} = R_f I_{q'} + L_f\frac{d}{dt}I_{q'} + \omega_s L_f I_{d'} + V_{q'} \end{cases} \tag{17}$$

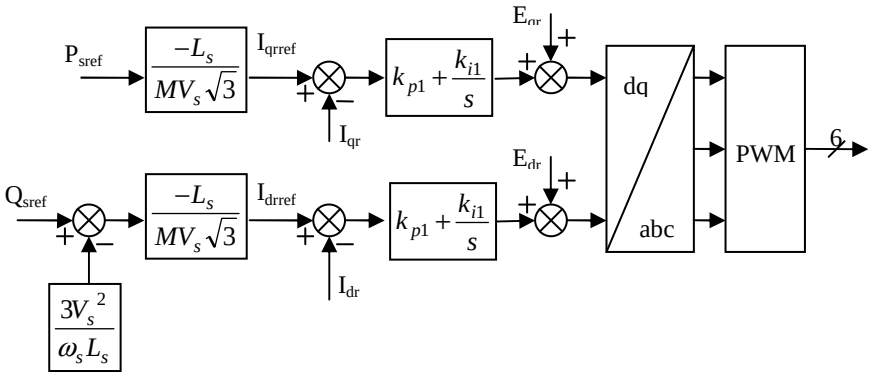

Fig. 6. RSC Vector Control.

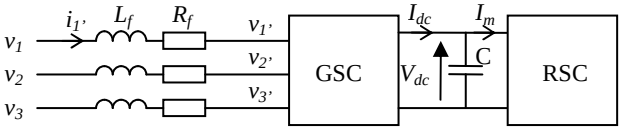

Fig. 7. GSC grid side connection.

After Laplace transformation, voltages defined by the equation (16) become:

$$\begin{cases} V_{ds}(s) = R_f I_{d'}(s) + L_f s I_{d'}(s) + E_{d'}(s) \\ V_{qs}(s) = R_f I_{q'}(s) + L_f s I_{q'}(s) + E_{q'}(s) \end{cases} \quad (18)$$

The resulting bloc diagrams for the voltages of the equation (18) are presented in the Fig. 8.

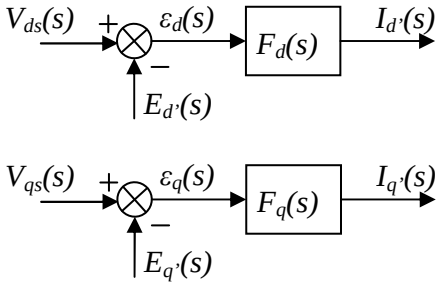

Fig. 8. Bloc diagrams for the GSC voltages.

With:

$$F_d(s) = F_q(s) = \frac{1}{R_f} \cdot \frac{1}{1 + \frac{L_f}{R_f} s} \quad (19)$$

The direct axis current is used to regulate the GSC reactive power Q_f and the quadrature axis current is used to regulate the DC bus voltage. This method also gives the possibility to control independently the active and reactive power echanged between the GSC and the electrical grid.

In the Park reference frame, the voltage source components are $V_{ds} = 0$ and $V_{qs} = V_s\sqrt{3}$ and the powers can be expressed by:

$$\begin{cases} P_f = V_s \sqrt{3} I_{q'} \\ Q_f = V_s \sqrt{3} I_{d'} \end{cases} \quad (20)$$

By neglecting the converter losses, we have:

$$\begin{cases} V_{dc} I_{dc} = V_s \sqrt{3} I_{q'} = P_f \\ C \dfrac{d}{dt} V_{dc} = I_{dc} - I_m \\ V_{dc} C \dfrac{d}{dt} V_{dc} = P_f - P_m \end{cases} \quad (21)$$

The GSC vector control diagram presented in the Fig. 9 is directly established from the equations (18) and (21) of the GSC model. We used a Proportional Integral corrector for the current and DC bus voltage controls [11].

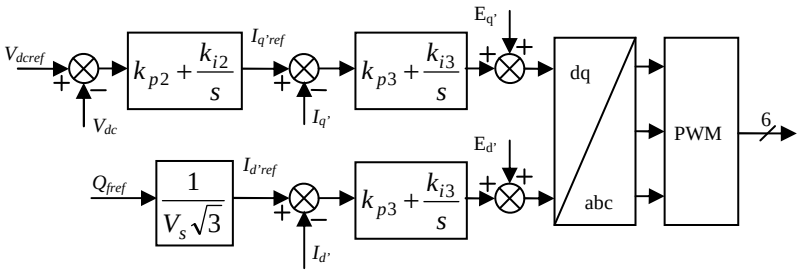

Fig. 9. GSC Vector Control.

VI. Simulation Results

In this section, we examine the response of the WECS in the four possible fault cases when a driver or a semiconductor is faulty. As explained in section III, only open switch fault is considered because of the use of fuses. We considered that the fault appears on the third leg of the RSC or of the GSC. The studied cases are the following:

- GSC is faulty in hypo synchronous mode (case *a*),
- GSC is faulty in hyper synchronous mode (case *b*),
- RSC is faulty in hypo synchronous mode (case *c*),
- RSC is faulty in hyper synchronous mode (case *d*).

Simulation results are obtained using Matlab/Simulink associated with the toolbox SymPowerSystems. System parameters are given in the Appendix. For the two cases *a* and *c*, speed generator Ω is regulated by MPPT at 140 rad/s and for cases *b* and *d*, the speed is equal to 200 rad/s.

VI.1. Fault occurrence without compensation

Fig. 10 and Fig. 11 present simulation results for the cases *a* and *b* respectively, when a fault of the top switch $T_{3'}$ of the GSC appears at t = 200 ms without fault detection.

Fig. 12 and Fig. 13 present simulation results for the cases *c* and *d* respectively, when a fault of the top switch T_3 of the RSC appears at t = 200 ms without fault detection.

For GSC fault occurrence in both speed conditions (cases *a* and *b)*, an open circuit without fault compensation leads to oscillations of the V_{dc} voltage and consequently of the power injected into the grid. We can notice that these oscillations are not the same in both speed conditions; in hypo synchronous mode, the GSC operates as a rectifier while in hyper synchronous mode it operates as an inverter.

For RSC fault occurrence in both speed conditions (cases *c* and *d*), we either observe oscillations of V_{dc} and consequently of P_{grid}. In hypo synchronous mode, the RSC operates as an inverter and consequently the grid power oscillations are not so important than in hyper synchronous mode where the RSC operates as a rectifier.

In conclusion, the four cases in any speed conditions lead to electrical and mechanical oscillations which dammage the WECS and the electrical grid.

VI.2. Fault occurrence with compensation

Fig. 14 and Fig. 15 present simulation results for the cases *a* and *b* respectively, when a fault of the top switch $T_{3'}$ of the GSC appears at t = 200 ms with fault detection and compensation.

Fig. 16 and Fig. 17 present simulation results for the cases *c* and *d* respectively, when a fault of the top switch T_3 of the RSC appears at t = 200 ms with fault detection and compensation.

With fault detection and compensation, WECS can still operate in nominal conditions. The fault is correctly detected in less than 10 µs. In the four cases, the fault is detected and the faulty leg of the GSC or the RSC is replaced by the redundant one.

VII. Conclusion

This paper validated the possibility to achieve fault tolerant operation for a WECS with DFIG by adding one redundant leg to the classical back-to-back power converter topology. More, we examined a new fault detection and compensation method, avoiding false fault detection due to semiconductor switching. The proposed method minimizes the delay time between the fault occurrence and the diagnosis. The simulation results demonstrate the possibility to detect a faulty switch in less than 10 µs by using a “time criterion” instead of “voltage criterion”. The lower limit for the detection time depends on the switching time. In actual WECS, when a fault appears on the back-to-back converter, the system is disconnected from the electrical grid. As proposed in this paper, with a fault tolerant back-to-back converter associated with fast fault detection and compensation, the WECS can still operate in nominal conditions and consequently economic benefits can be realized. More, the fault detection principle detailed in this paper can be used in any application using three-phase voltage source inverter.

We are currently working on fault tolerant WECS with DFIG when a voltage or a current sensor is faulty to increase the reliability of this green power generation system.

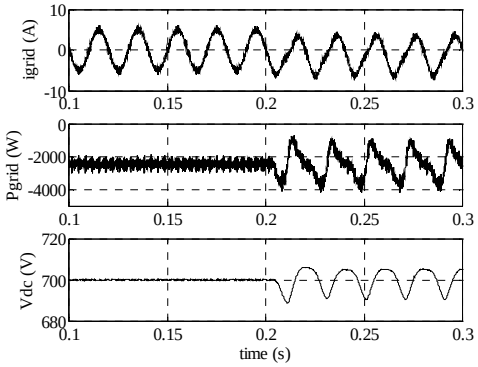

Fig. 10. Case *a* without fault compensation

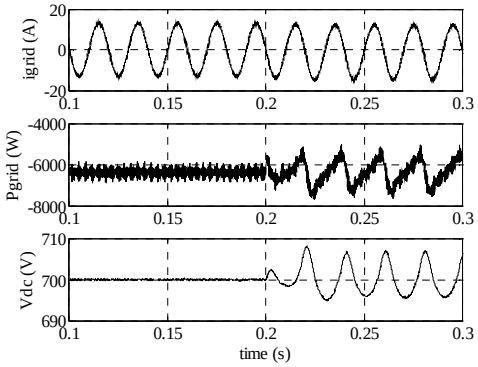

Fig. 11. Case *b* without fault compensation

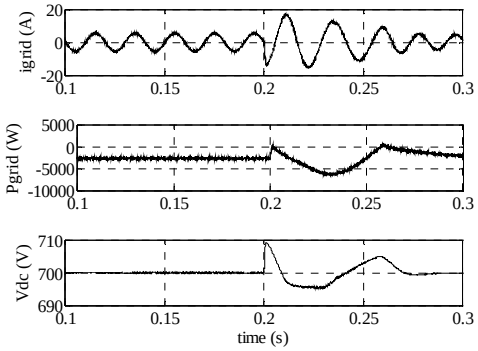

Fig. 12. Case *c* without fault compensation

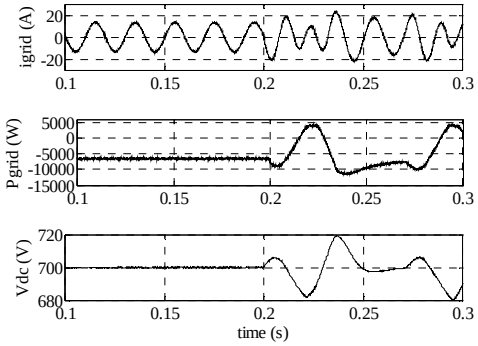

Fig. 13. Case *d* without fault compensation

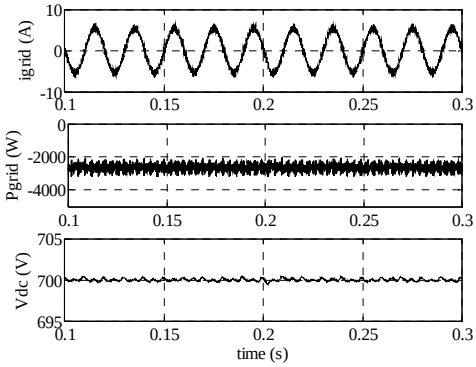

Fig. 14. Case *a* with fault compensation

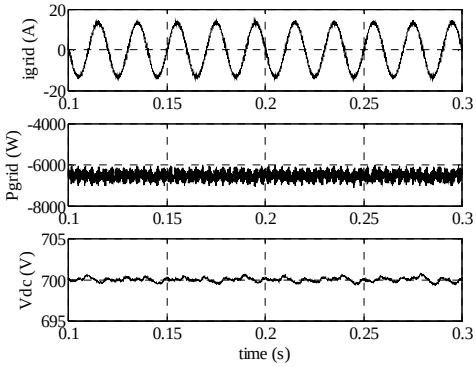

Fig. 15. Case *b* with fault compensation

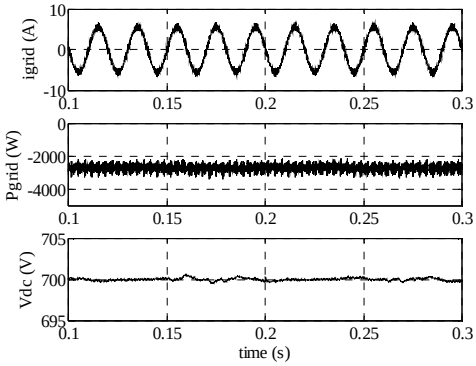

Fig. 16. Case *c* with fault compensation

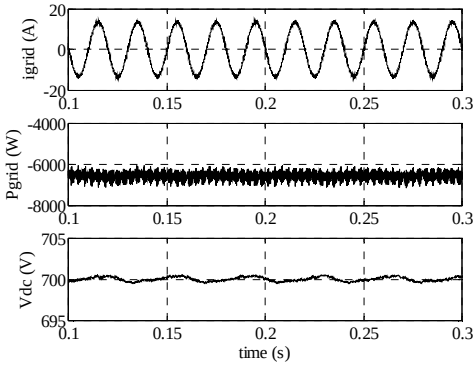

Fig. 17. Case *d* with fault compensation

Appendix

Grid parameters: 230V-50Hz, V_s=230V, ω_s=314rad/s

DFIG parameters: R_s=0.455Ω, R_r=0.19 Ω, L_s=70mH, L_r=21mH, M=34mH, σ=0.214, f=0.00673Nm/rad/s, J=0.3125kg.m^2

$$E_{ds} = \frac{M}{L_r}V_{dr} - \frac{MR_r}{L_r}I_{dr} + (\omega_r - \omega_s)MI_{qr} + \left(\frac{M^2}{L_r}\omega_r - L_s\omega_s\right)I_{qs}$$

$$E_{qs} = \frac{M}{L_r}V_{qr} - \frac{MR_r}{L_r}I_{qr} + (\omega_s - \omega_r)MI_{dr} + \left(L_s\omega_s - \frac{M^2}{L_r}\omega_r\right)I_{ds}$$

$$E_{dr} = \frac{M}{L_s}V_{ds} - \frac{MR_s}{L_s}I_{ds} + (\omega_s - \omega_r)MI_{qs} + \left(\frac{M^2}{L_s}\omega_s - L_r\omega_r\right)I_{qr}$$

$$E_{qr} = \frac{M}{L_s}V_{qs} - \frac{MR_s}{L_s}I_{qs} + (\omega_r - \omega_s)MI_{ds} + \left(L_r\omega_r - \frac{M^2}{L_s}\omega_s\right)I_{dr}$$

Filter and DC bus capacitance parameters: R_f=1m Ω, L_f=4mH, C=600µF

RSC Vector Control: P_{sref}=-6kW at Ω=200rad/s, P_{sref}=-10 kW at Ω=140rad/s, Q_{sref}=0VAr, k_{p1}=13.482, k_{i1}=570

GSC Vector Control: V_{dcref}=700V, I_{dsref}=0A, k_{p2}=0.229, k_{i2}=43.74, k_{p3}=12, k_{i3}=3

References

[1] R. Billinton, B. Guang, "Generating capacity adequacy associated with wind energy", *IEEE transactions on wind energy conversion*, Volume 19, Issue 3, Sept. 2004, pp. 641 – 646.

[2] V. Van Thong, R. Belmans, Distributed Generation Overview: Current Status and Challenges, *International Review of Electrical Engineering (IREE)*, April 2006.

[3] S. Skander-Mustapha, I. Slama-Belkhodja, Current Sensor Failure in a DFIG Wind-Turbine: Effect Analysis, Detection and Control Reconfiguration, *International Review of Electrical Engineering (IREE)*, August 2006.

[4] D. Kastha and B. KJ. Bose, "Investigation of fault modes of voltage-fed inverter system for induction motor drive", *IEEE Transactions on Industry Applications*, 1994, vol. 30, pp. 1028-1038.

[5] R. Peuget, S. Courtine, J. Rognon, "Fault detection and isolation on a PWM inverter by knowledge-based model", *IEEE Transactions on Industry Applications*, 1998, vol. 34, pp. 1318-1325.

[6] A.M.S. Mendes, A.J.M. Cardoso, "Fault diagnosis in a rectifier –inverter system used in variable speed AC drive, by the average current Park's vector approach", *European Power Electronics Conference, Lausanne*, 1999, pp. 1-9.

[7] C. Karl, K. Kafka, "Power electronics monitoring for a controlled voltage source inverter drive with induction machines", *Proceedings IEEE Power Electronics Specialists Conference*, 2000.

[8] R.L.A. Ribeiro, C.B. Jacobina, E.R.C. da Silva, A.M.N. Lima "Fault detection in voltage-fed PWM motor drive systems", *IEEE IAS Annual Meet.*, 2000, vol. 1, pp.242-247.

[9] T. Ghennam, E. M. Berkouk, B. Francois , A Vector Hysteresis Current Control Applied on Three-Level Inverter. Application to the Active and Reactive Power Control of Doubly Fed Induction Generator Based Wind Turbine, *International Review of Electrical Engineering (IREE)*, April 2007.

[10] A. Boyette, P. Poure, S. Saadate, "Direct and indirect control of a Doubly Fed Induction Generator wind turbine including a storage unit", *32th Annual Conference of the IEEE Industrial Electronics Society*, November, 2006, Paris, France.

[11] C. Belfedal, S. Moreau, G. Champenois, T. Allaoui, M. Denai, Comparison of PI and Direct Power Control with SVM of Doubly Fed Induction Generator, *International Review of Electrical Engineering (IREE)*, August 2006.

Authors' information

[1] Groupe de Recherches en Electrotechnique et Electronique de Nancy UMR 7037, Nancy-Université, CNRS - Faculté des Sciences et Techniques - BP 239 - 54506 Vandoeuvre Cedex - France

[2]Laboratoire d'Instrumentation Electronique de Nancy EA 3440, Nancy-Université- CNRS - Faculté des Sciences et Techniques – BP 239 - 54506 Vandoeuvre Cedex - France

Arnaud GAILLARD was born in Epinal, France, in 1982. He received the M. Sc. Degree in Electrical Engineering from the University Henri Poincaré of Nancy I, France in 2006. He is currently working toward the Ph.D degree in Electrical Engineering at UHP of Nancy I, GREEN laboratory. His research interests include fault tolerant converters, power quality and wind energy conversion systems.

Shahram KARIMI was born in Kermanshah, Iran, in 1972. He received the B.S. degree in electrical engineering from Tabriz university, Tabriz, Iran, in 1995, the M.S. degree in electrical engineering from Sharif university, Tehran, Iran, in 1997. He joined the Gharb High Education and Research Institute, Kermanshah, Iran, in 1999, and is currently pursuing the Ph.D. degree in the GREEN-UHP, Nancy, France. His research interests are active power filters, power quality and fault tolerant converters.

Philippe POURE was born in 1968. He received the Engineer Degree and Ph.D. Degree in Electrical Engineering from INPL-ENSEM-GREEN, France, in 1991 and 1995 respectively. Since 1995, he is an Associate Professor and worked first at the University Louis Pasteur of Strasbourg, France, in the field of mixed-signal System-On-Chip for control and measurement in Electrical Engineering. Since September 2004, he joined the University Henri Poincaré – Nancy I, France and works on power quality, more particularly on active filtering and wind energy conversion systems.

Shahrokh SAADATE was born in Teheran/IRAN on May 5th, 1958, received his engineer degree in 1982, his Master of research in 1982, his PHD thesis in 1986 and his "Habilitation à diriger des recherches" in 1995 from INPL-ENSEM Nancy, FRANCE. Currently, he is Professor in Electrical Engineering in the University Henri Poincaré – Nancy I, France, GREEN laboratory. His main research domains are power electronics and systems, power quality and wind energy conversion.